More than Meets the Eye - A Portable Measurement Unit for Characterizing Light Energy Availability

John Sarik, Kanghwan Kim, Maria Gorlatova, Ioannis Kymissis, Gil Zussman
Electrical Engineering, Columbia University, New York, NY, 10027
{jcs2160, kk2885, mag2206}@columbia.edu, {johnkym, gil}@ee.columbia.edu

***Abstract*—Characterizations of environmental energy availability and properties provide important insights for designing energy harvesting nodes and developing energy harvesting adaptive systems and algorithms. Previous characterizations of light energy availability provided baseline estimates of the total available energy that could be harvested by a crystalline silicon solar cell. However, these measurements *did not consider the spectral composition of the incident light*. In this paper, we present a method and a proof-of-concept implementation for obtaining information about the spectral composition of the incident light. LightBox, a portable measurement unit, determines the light source, measures the incident irradiance, and calculates the amount of energy that would be harvested by two different harvesters: a crystalline silicon solar cell and an amorphous silicon solar cell. To the best of our knowledge, LightBox is *the first portable irradiance measurement device that considers the spectral composition of the incident light*. Our method and proof-of-concept implementation are an important step toward better characterizing environmental light energy availability for energy harvesting nodes deployed in a wide range of environments. The insights from this data will enable the development and wide deployment of energy-aware algorithms and systems.**

***Index Terms*—Energy harvesting, light energy characterization, spectral intensity distribution, solar cells.**

I. Introduction

Advances in energy harvesting and ultra-low power communication technologies have enabled energetically self-reliant wireless nodes [7], [13] that require *energy harvesting adaptive communications and networking*. Energy harvesting-aware protocols that account for the expected environmental energy, deterministically or stochastically, allow networks to adapt to efficiently spend the energy [6], [12]. Developing such protocols requires experimental characterization of the energy available from the environments in which the nodes will be deployed. Initial characterizations of environmental light energy availability have been conducted and provide first-order estimates of the available energy [5]. However, these estimates implicitly assume that the harvester is a crystalline silicon solar cell, while future energy harvesting networks are likely to rely on a range of solar cell technologies, including amorphous silicon [13] and organic photovoltaics [3].

Determining the energy harvested by different solar cells requires knowledge of the *spectral composition* of the incident light. Fig. 1 shows the normalized spectral distribution, $\bar{E}_e(\lambda)$, of different common indoor light sources. It is important to note that *the overall efficiency of the harvester depends on the spectral composition of the incident light.* For example, a crystalline silicon solar cell will harvest more energy than an amorphous silicon solar cell under outdoor illumination, but the amorphous silicon solar cell will harvest more energy under an LED light source [1]. If the energy availability estimates from [5] are used, energy harvesting nodes equipped with amorphous silicon solar cells may underestimate the available energy indoors and overestimate the available energy outdoors, resulting in suboptimal energy use.

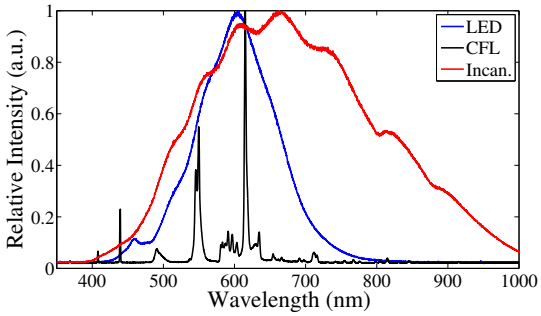

Fig. 1. Normalized spectral distribution of three different light sources: incandescent, compact fluorescent (CFL), and LED.

Additionally, accurately measuring the environmental energy available to *portable nodes* (such as mobile and wearable nodes) requires a portable measurement device, while compact diffraction grating spectrometers that can be used to measure the complete light spectrum must be connected to a PC. However, it is not necessary to measure the *complete* spectrum of the incident light. If there is a single dominant light source, the light source can be identified using a series of photodetectors with different responsivities. For example, it is easy to distinguish between sunlight and indoor light using an infrared (IR) photodetector because sunlight has a strong IR component that is not present in artificial light sources [9]. Similarly, it is possible to use a combination of photodetectors to identify distinguishing components of artificial light sources. This approach has been used previously to determine the color temperature, but not the spectral composition, of a light source [10]. Based on this principle, we developed LightBox: a portable, low-cost measurement unit that determines the spectral composition of the incident light and measures the incident irradiance. The measurements collected by LightBox provide more accurate estimates of energy availability, especially for mobile nodes that will be exposed to both indoor and outdoor conditions.

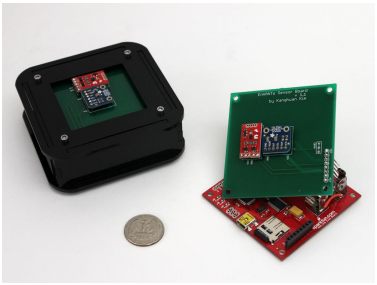

Fig. 2. The proof-of-concept LightBox measurement unit.

II. LightBox System Description

The LightBox portable light energy measurement unit measures and logs the output of two low-cost, multichannel light sensors. This information is then used to determine the spectral composition of the incident light source, calculate the incident irradiance, and estimate the amount of energy that can be harvested by different solar cells under this illumination. We can calculate c, the expected output of a channel, using the following equation:

$$c = \int_0^\infty E_e(\lambda)R(\lambda)d\lambda, \tag{1}$$

where $E_e(\lambda)$ is the spectral irradiance of the incident light source in W/cm^3 and $R(\lambda)$ is the responsivity of the channel in counts/(W/cm^2). This equation can be rewritten as:

$$c = E_e R \int_0^\infty \bar{E}_e(\lambda)\bar{R}(\lambda)d\lambda, \tag{2}$$

where E_e is the incident irradiance in W/cm^2, R is a conversion factor with units counts/(W/cm^2), $\bar{E}_e(\lambda)$ is the normalized spectral distribution of the incident light source, and $\bar{R}(\lambda)$ is the normalized responsivity of the channel. It is important to note that the ratio of the *output of two channels depends on the normalized spectral distribution of the incident light source but not on the incident irradiance*. Therefore, we can classify the light source by using *the ratios of different channels*. After the light source has been determined, we can calculate the incident irradiance as $E_e = c/R_0$, where $R_0 = R\int_0^\infty \bar{E}_e(\lambda)\bar{R}(\lambda)d\lambda$. For a given channel, this factor will be different depending on the incident light source.

A LightBox, shown in Fig. 2, consists of a Sparkfun ADXL345 evaluation board with an Atmel ATMega328P microprocessor, a microSD card for data logging, an Avago ADJD-S371 RGB digital color sensor, and a TAOS TSL2561 light-to-digital converter. The operation of the LightBox is shown schematically in Fig. 3. The ADJD-S371 color sensor provides four readings: the intensity of light through a red filter (R), green filter (G), blue filter (B), and clear filter (C). The TSL2561 light-to-digital converter provides two readings: full spectrum (FS) intensity and infrared (IR) light intensity. The spectral responsivity, $R(\lambda)$, of the different channels is shown in Fig. 4. Data from the six channels is logged to the microSD card every second.

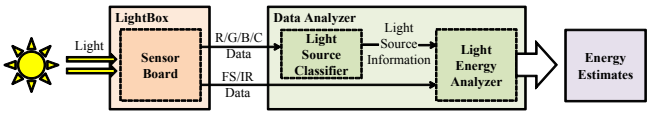

Fig. 3. The schematic representation of the LightBox spectral determination and energy estimation process.

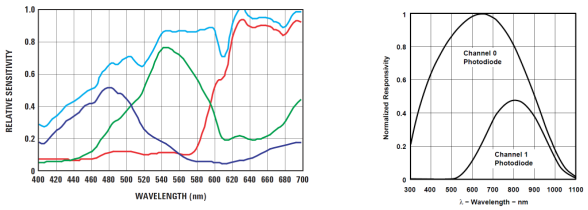

(a) (b)

Fig. 4. (a) Spectral response of the color light sensor (taken from [11]), and (b) spectral response of the full spectrum light sensor (taken from [2]).

III. Light Source Classifier

Our proof-of-concept system demonstrates light source classification using the ratios of different channel counts as a feature vector. Specifically, the classifier feature space is the ratios of R, G, and B channel outputs to the C channel output. This feature space and the decision boundaries for a particular classifier (see below) are shown in Fig. 5.

A fully controlled experimental setup was built to obtain an accurately labeled training and test data for the classification and to demonstrate the LightBoxes "in action". The setup is shown in Fig. 6. It consists of light-proof enclosures that replicate different indoor light environments. We experimented with 3 particular light sources: incandescent, compact fluorescent, and LED light bulbs. We use this setup to demonstrate that LightBoxes can distinguish light conditions that are *indistinguishable to the human eye*. Specifically, when we use light bulbs of similar color temperature, humans cannot identify the different light sources using only the naked eye, while they are clearly distinguishable in the processed LightBox outputs.

We used a simple minimum-distance Maximum Likelihood (ML) classifier. While we experimented with several other classifiers (such as the Kth Nearest Neighbor, Support Vector Machine, and Relevance Vector Machine classifiers), we ulti-

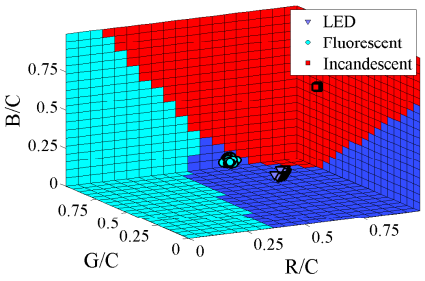

Fig. 5. The light source classifier feature space, and the decision boundaries and test data points for the Maximum Likelihood classifier we implemented in the portable measurement unit.

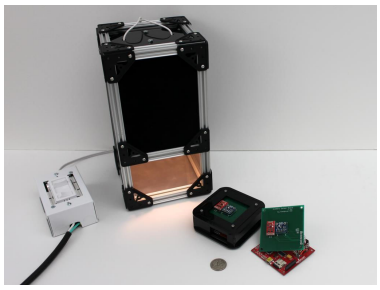

Fig. 6. The setup developed to experiment with light source classifiers.

mately chose the ML classifier because of its simplicity. The classifier operates as follows. First, using the training data set, we calculate the center of mass for all the data points for each light source in the feature space. To classify an unknown light source measured by LightBox, we find the light source type for which the Euclidian distance of the measurement's feature vector is minimized. For each light source, we obtained 100 training data points and 100 test data points over a wide range of incident irradiance. With the 300 data points representing 3 different single-source light conditions, the classifier correctly identified the energy source *more than 98% of the time*.

Our preliminary experiments with light traces captured by carrying a LightBox in *natural* environments indicate a low rate of misclassifications when only a single dominant energy source is present. In the presence of multiple light sources, such as in a sunlit office, the classifier may not function well because the spectral mixture of different light sources may closely resemble a different light source. One potential extension is developing an experimental setup to precisely recreate mixed-source conditions to determine suitable mixture models and classifiers for such conditions.[1]

IV. Energy Availability Estimates

Two important metrics for photovoltaic energy harvesting systems are the total available environmental energy (incident irradiance) and the total energy harvested by a specific solar cell. The instantaneous power generated by a solar cell can be calculated using the following equation:

$$P_{sc} = A_{sc} V_{sc} \int_0^\infty R_{sc}(\lambda) E_e(\lambda) d\lambda, \tag{3}$$

where A_{sc} is the area of the solar cell in cm^2, V_{sc} is the operating voltage of the solar cell in V, R_{sc} is the spectral responsivity of the solar cell in A/W, and $E_e(\lambda)$ is the spectral irradiance of the incident light source in W/cm^3. For a given light source this can be rewritten in terms of counts measured by a channel, c, as

$$P_{sc} = \eta E_e = \eta c / R_0, \tag{4}$$

[1]We note that obtaining the "ground truth" information about the intensity and spectral composition of the light in multi-source conditions is difficult. Typically, the light incident on a harvester will be a low-intensity, diffuse combination of light generated by multiple sources and reflected by multiple surfaces. Due to the low sensitivity of diffraction grating spectrometers, it is not possible to concentrate this low-intensity, diffuse light and measure its spectral composition in real time.

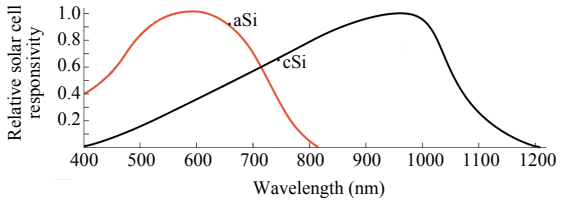

Fig. 7. Spectral response of amorphous silicon (aSi) and crystalline silicon (cSi) solar cells (adapted from [8]).

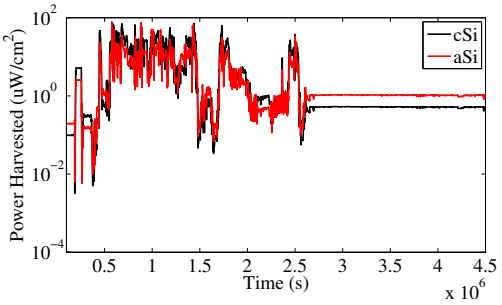

Fig. 8. Trace of the estimated energy harvested by different solar cells.

where $\eta = A_{sc} V_{sc} \int_0^\infty R_{sc}(\lambda) \bar{E}_e(\lambda) d\lambda$ is the overall efficiency of the solar cell. In previous work [5] instantaneous power was calculated using the same factors η and R_0 for all light sources. This gives an accurate estimate of the energy harvested by a solar cell if the spectral responsivity of the sensor and the solar cell are similar (for example, the measurements collected with a silicon photodetector accurately estimate the energy that could be harvested by a crystalline silicon solar cell). By determining the spectral composition of the incoming light, the measurements collected by our sensors can be used to determine the amount of energy that could be harvested by a solar cell with an arbitrary responsivity.

The normalized spectral responsivity, $\bar{R}_{sc}$, of a crystalline silicon solar cell (cSi) and an amorphous silicon cell (aSi) are shown in Fig. 7. The cSi solar cell has a spectral sensitivity range of 500nm to 1100nm and is well suited to harvesting energy from solar illumination which has a strong IR component. The aSi solar cell has a spectral sensitivity range of 300nm to 700nm and is well suited to harvesting energy from artificial light sources that generate light in the visible range.

We collected a series of traces from a LightBox attached to a student's bag. An example trace collected by a LightBox is shown in Fig. 8. To process the data, we assume two possible harvesters: a cSi solar cell where $\eta = 10\%$ under outdoor illumination and $\eta = 5\%$ under indoor illumination and an aSi solar cell where $\eta = 5\%$ under outdoor illumination and $\eta = 10\%$ under indoor illumination. It is possible to conduct more sophisticated processing, but even this first order approximation provides useful insights into the energy harvesting process. The results for eight traces are summarized in Table I.

Trace 1 was recorded almost exclusively outdoors, traces 2-4 include a combination of indoor and outdoor activities,

TABLE I
TRACE DATA COLLECTED BY LIGHTBOX.

#	Duration	Average irradiance (mJ/cm^2)	Average power (μW/cm^2)	
			cSi	aSi
1	1h 23m 59s	1211.3	119.5	62.2
2	2h 08m 35s	460.4	39.5	29.7
3	1h 36m 22s	451.3	39.4	28.3
4	2h 24m 35s	474.8	41.6	29.6
5	1h 56m 13s	158.9	8.0	15.8
6	1h 39m 45s	95.3	5.3	9.0
7	1h 18m 17s	80.1	4.2	7.9
8	1h 08m 11s	68.3	3.7	6.5

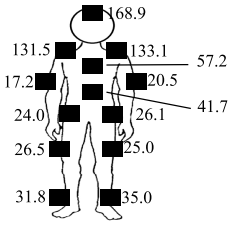

Fig. 9. Irradiance measurements (μW/cm^2) from different locations on the body demonstrating the spatial variability of energy availability.

and traces 5-8 were recorded almost exclusively indoors. As expected, the irradiance seen by exclusively indoor nodes is on the order of 100μW/cm^2 and the irradiance seen by outdoor nodes is up to two orders of magnitude greater. Trace 2 demonstrates the usefulness of determining the spectral composition of the light. Without the spectral information, we would assume that the entire trace was recorded outdoors. If our harvester was an aSi solar cell, we would assume $\eta = 5\%$ for the entire trace, but that would cause us to *underestimate the average power generated by 22%*. Similarly, if our harvester was a cSi solar cell and we assumed $\eta = 10\%$ for the entire trace, we would *overestimate the average power generated by 15%*.

We also used the portability of the LightBox to explore the *spatial variations* of energy availability, which is especially important for *wearable* nodes. Fig. 9 shows the measurements of average irradiance for different placements of Lightbox on a stationary person who is standing directly underneath an overhead lamp. While the often-cited rule-of-thumb estimate of energy availability for indoor environments is 100μW/cm^2 incident irradiance, it can be seen that the available energy for a wearable node may be up to 60% greater or 80% less depending on its placement.

V. CONCLUSIONS AND FUTURE WORK

While energy harvesting and low-power wireless communications are becoming ubiquitous, there are many low-layer challenges in understanding the *energy availability* for these nodes. Specifically, existing light energy availability measurements only considered the overall irradiance of the incident light and not its spectral composition. We developed a proof-of-concept LightBox system, a portable system that uniquely considers the spectral composition of the incident light, which enables better estimates of energy availability, especially for systems that use different solar cell technologies. Future versions of LightBox could include an onboard classifier to simplify data gathering and processing. LightBox could also use different light sensors specifically designed to identify features of common indoor light sources.

The current version of LightBox additionally includes a tri-axis accelerometer, and can be used to simultaneously measure *light* and *motion* energy availability.[2] This will enable system designers to determine the best energy source for their application or to develop energy harvesting-aware multi-harvester systems. Another extension is to develop a smaller, wearable version of LightBox. This will enable more measurements and provide insight into how the spatial variation of energy availability changes during different activities. Better understanding environmental energy availability for energy harvesting nodes deployed in a wide range of environments will enable smarter, more efficient deployments.

VI. ACKNOWLEDGEMENTS

This work was supported in part by the Vodafone Americas Foundation Wireless Innovation Project and NSF grants CCF-0964497 and CNS-1054856.

REFERENCES

[1] Y. Afsar, J. Sarik, M. Gorlatova, G. Zussman, and I. Kymissis. Evaluating photovoltaic performance indoors. In *Proc. IEEE PVSC'12*, July 2012.
[2] Avago Technologies. ADJD-S311-CR999 miniature surface mount RGB digital color sensor, July 2007.
[3] M. Gorlatova, R. Margolies, J. Sarik, G. Stanje, J. Zhu, B. Vigraham, M. Szczodrak, L. Carloni, P. Kinget, I. Kymissis, and G. Zussman. Prototyping energy harvesting active networked tags (EnHANTs). In *Proc. IEEE INFOCOM'13 mini-conference*, Apr. 2013.
[4] M. Gorlatova, J. Sarik, M. Cong, K. Kim, I. Kymissis, and G. Zussman. Movers and shakers: Kinetic energy harvesting for the Internet of Things. Technical Report arXiv:1307.0044, July 2013.
[5] M. Gorlatova, A. Wallwater, and G. Zussman. Networking low-power energy harvesting devices: Measurements and algorithms. *IEEE Transactions on Mobile Computing*, 12(9), Sept. 2013.
[6] L. Huang and M. Neely. Utility optimal scheduling in energy harvesting networks. In *Proc. ACM MobiHoc'11*, May 2011.
[7] V. Raghunathan, A. Kansal, J. Hsu, J. Friedman, and M. Srivastava. Design considerations for solar energy harvesting wireless embedded systems. In *Proc. IEEE IPSN'05*, Apr. 2005.
[8] Sanyo. Amorphous silicon solar cells / amorphous photosensors. Available at us.sanyo.com/Dynamic/customPages/docs/solarPower_Amorphous_PV_Product_Brochure_EP120B.pdf, Nov. 2007.
[9] J. Smith. Ambient light sensing (ALS), Mar. 2009.
[10] J. Smith. Calculating color temperature and illuminance using the TAOS TCS3414CS digital color sensor, Feb. 2009.
[11] TAOS. TSL2560, TSL2561 Light-To-Digital Converter, Dec. 2005.
[12] J. Yang, O. Ozel, and S. Ulukus. Broadcasting with a battery limited energy harvesting rechargeable transmitter. In *Proc. IEEE WiOpt'11*, 2011.
[13] L. Yerva, A. Bansal, B. Campbell, T. Schmid, and P. Dutta. Grafting energy-harvesting leaves onto the sensornet tree. In *Proc. IEEE IPSN'12*, Apr. 2012.

[2]Obtaining motion energy availability estimates from acceleration data is detailed in, for example, [4].